Brain region-specific amyloid plaque-associated myelin lipid loss, APOE deposition and disruption of the myelin sheath in familial Alzheimer's

Downloaded from: https://research.chalmers.se, 2026-04-03 01:38 UTC

Citation for the original published paper (version of record):

Kaya, I., Jennische, E., Lange, S. et al (2020). Brain region-specific amyloid plaque-associated myelin lipid loss, APOE deposition and
disruption of the myelin sheath in familial Alzheimer's disease mice. Journal of Neurochemistry, 154(1): 84-98. http://dx.doi.org/10.1111/jnc.14999

N.B. When citing this work, cite the original published paper.

research.chalmers.se offers the possibility of retrieving research publications produced at Chalmers University of Technology. It covers all kind of research output: articles, dissertations, conference papers, reports etc. since 2004. research.chalmers.se is administrated and maintained by Chalmers Library

(article starts on next page)

Received: 26 December 2019 | Revised: 7 February 2020 | Accepted: 2 March 2020

DOI: 10.1111/jnc.14999

Check for updates

ORIGINAL ARTICLE

Journal of Neurochemistry JNC The Official Journal of the International Society for Neurochemistry WILEY

Brain region-specific amyloid plaque-associated myelin lipid loss, APOE deposition and disruption of the myelin sheath in familial Alzheimer's disease mice

Ibrahim Kaya[1,2] | Eva Jennische[3] | Stefan Lange[3] | Ahmet Tarik Baykal[4] | Per Malmberg[5] | John S. Fletcher[2]

[1]Department of Psychiatry and Neurochemistry, Sahlgrenska Academy at the University of Gothenburg, Mölndal, Sweden

[2]Department of Chemistry and Molecular Biology, University of Gothenburg, Gothenburg, Sweden

[3]Institute of Biomedicine, University of Gothenburg, Gothenburg, Sweden

[4]Department of Medical Biochemistry, Faculty of Medicine, Acibadem Mehmet Ali Aydinlar University, Istanbul, Turkey

[5]Department of Chemistry and Chemical Engineering, Chalmers University of Technology, Gothenburg, Sweden

Correspondence
Ibrahim Kaya and John S. Fletcher, Department of Chemistry and Molecular Biology, University of Gothenburg, Analytical, Chemistry, Plan 4, Kemigården 4, SE-412 96, Gothenburg, Sweden.
Email: ibrahim.kaya@neuro.gu.se; john.fletcher@chem.gu.se

Funding information
LUA/ALF; Sahlgrenska University Hospital; Swedish Research Council; Knut and Alice Wallenberg Foundation; USA National Institutes of Health (NIH); European Research Council (ERC); The Scientific and Technological Research Council of Turkey (TUBITAK)

Abstract

There is emerging evidence that amyloid beta (Aβ) aggregates forming neuritic plaques lead to impairment of the lipid-rich myelin sheath and glia. In this study, we examined focal myelin lipid alterations and the disruption of the myelin sheath associated with amyloid plaques in a widely used familial Alzheimer's disease (AD) mouse model; 5xFAD. This AD mouse model has $A\beta_{42}$ peptide-rich plaque deposition in the brain parenchyma. Matrix-assisted laser desorption/ionization imaging mass spectrometry of coronal brain tissue sections revealed focal Aβ plaque-associated depletion of multiple myelin-associated lipid species including sulfatides, galactosylceramides, and specific plasmalogen phopshatidylethanolamines in the hippocampus, cortex, and on the edges of corpus callosum. Certain phosphatidylcholines abundant in myelin were also depleted in amyloid plaques on the edges of corpus callosum. Further, lysophosphatidylethanolamines and lysophosphatidylcholines, implicated in neuroinflammation, were found to accumulate in amyloid plaques. Double staining of the consecutive sections with fluoromyelin and amyloid-specific antibody revealed amyloid plaque-associated myelin sheath disruption on the edges of the corpus callosum which is specifically correlated with plaque-associated myelin lipid loss only in this region. Further, apolipoprotein E, which is implicated in depletion of sulfatides in AD brain, is deposited in all the Aβ plaques which suggest apolipoprotein E might mediate sulfatide depletion as a consequence of an immune response to Aβ deposition. This high-spatial resolution matrix-assisted laser desorption/ionization imaging mass spectrometry study in combination with (immuno) fluorescence staining of 5xFAD mouse brain provides new understanding of morphological, molecular and immune signatures of Aβ plaque pathology-associated myelin lipid loss and myelin degeneration in a brain region-specific manner.

Abbreviations: AD, Alzheimer's disease; APOE, apolipoprotein E; APP, Aβ precursor protein; Aβ, amyloid beta; CA, cornu ammonis; Cer, ceramides; DAN, diaminonapthalene; DG, dentate gyrus; FAD, familial AD; GalCer, galactosylceramides; gcl, granular cell layer; GFAP, glial fibrillary acidic protein; LPC, lysophosphatidylcholine; LPE, lysophosphatidylethanolamine; MALDI, matrix-assisted laser desorption/ionization; PE, phosphatidylethanolamine; pl, pyramidal cell layer; PSEN, presenilin; SAD, sporadic AD; ST, sulfatides; TREM 2, triggering receptor expressed on myeloid cells 2

Read the Editorial Highlight for this article on https://doi.org/10.1111/jnc.15025

This is an open access article under the terms of the Creative Commons Attribution License, which permits use, distribution and reproduction in any medium, provided the original work is properly cited.
© 2020 The Authors. *Journal of Neurochemistry* published by John Wiley & Sons Ltd on behalf of International Society for Neurochemistry

KEYWORDS
Alzheimer's disease, amyloid plaques, apolipoprotein E (APOE), MALDI Imaging Mass Spectrometry, myelin lipids, sulfatides

1 | INTRODUCTION

According to the amyloid hypothesis, accumulation of amyloid beta (Aβ) plays a central and causative part in Alzheimer's disease (AD) pathogenesis and the rest of the disease process (Hardy & Higgins, 1992). Aβ aggregates into oligomers that form diffuse and neuritic plaques in the brain parenchyma, which have been suggested to cause dysfunction and loss of neurons and synapses (Lacor et al., 2004; Palop & Mucke, 2010). However, there is also emerging evidence that this process may lead to impairment of the lipid-rich myelin sheath and the oligodendrocyte degeneration present in the brains of AD patients and transgenic AD mice models (Behrendt et al., 2013; Desai, Guercio, Narrow, & Bowers, 2011; Nasrabady, Rizvi, Goldman, & Brickman, 2018). The presence of intracellular granular lipid deposits in multiple cell types and myelin deficits in the brain parenchyma in AD was initially described by Aloysius Alzheimer in 1911 (Foley, 2010; Möller & Graeber, 1998). Further, the E4 allelic variant of the apolipoprotein (APOE) gene which encodes a protein involved in the sterol and sphingolipid metabolism such as the modulation of sulfatide content, and lipid transport (Bu, 2009; Han, Cheng, Fryer, Fagan, & Holtzman, 2003; Kim, Basak, & Holtzman, 2009) was suggested to be a prominent risk factor for sporadic AD and late-onset familial AD (FAD) (Corder et al., 1993; Saunders et al., 1993; Strittmatter et al., 1993). APOE linked the aberrant lipid biochemistry to AD pathogenesis in postmortem human AD and transgenic AD mice brains (Bandaru et al., 2009; Han, M. Holtzman, W. McKeel, Kelley, & Morris, 2002). Therefore, the role of intracellular lipid deposits, lipid biochemistry and myelin disruption in association with amyloid pathology in AD pathogenesis has been widely scrutinized (Bartzokis, 2004; Collins-Praino et al., 2014; Di Paolo & Kim, 2011; Mitew et al., 2010; Palavicini et al., 2017; Yang et al., 2014). Morphological data from human presenilin-1 familial, sporadic and preclinical AD cases, as well as in aged transgenic mice models, tg2576 ($APP_{Swe\ 670/671}$) and APP/PS1 (APP_{Swe} · $PS1_{M146L}$) has revealed a clear association between the fibrillary Aβ pathology and focal disruption of the myelin sheath in the gray matter of the neocortex compared with the age-matched control tissue (Mitew et al., 2010). Moreover, there was a focal loss of oligodendrocytes in sporadic and preclinical AD cases (Mitew et al., 2010) which is in line with the finding that amyloid-β peptides are cytotoxic to oligodendrocytes (Xu et al., 2001). However, molecular aspects of these observations still remain unknown.

Early lipidomics studies using brain tissue extracts revealed that sulfatides and plasmalogens substantially and specifically deplete, while ceramides elevate at the very early stages of AD (Han, Holtzman, & McKeel, 2001a; Han et al., 2002). Further, a body of evidence deduced from shotgun lipidomic analysis of brain tissue extracts suggested that APOE mediates sulfatide depletion in APP transgenic mice models (Cheng, Zhou, Holtzman, & Han, 2010). However, there was no direct correlation between sulfatide depletion and amyloid plaque-associated pathology. While recent data has revealed focal depletion of several sulfatide species in the amyloid plaques in the hippocampus and cerebral cortex of the brain in transgenic AD mice models, tgArcSwe ($APP_{E693G(Arctic)/KM670/671NI(Swedish)}$) (Kaya, Brinet, Michno, Başkurt, et al., 2017; Kaya, Brinet, Michno, Syvänen, et al., 2017) and tgSwe ($APP_{KM670/671NI}$) (Michno et al., 2018), it still remains unknown whether these observations are associated with myelin disruption and/or other factors such as APOE in association with amyloid plaques in specific brain regions.

Matrix-assisted laser desorption/ionization imaging mass spectrometry (MALDI-IMS) offers high-throughput spatial interrogation of the relative abundances of many lipid species on the surfaces of tissue sections (McDonnell & Heeren, 2007; Zemski Berry et al., 2011). MALDI-IMS has been widely used to probe the altered spatial lipid biochemistry in brain diseases including AD (Caughlin et al., 2018; Hamilton et al., 2015; Hong et al., 2016; Kaya, Zetterberg, Blennow, Hanrieder, & r., 2018b; Yuki et al., 2014), Huntington's disease (Hunter, Demarais, Faull, Grey, & Curtis, 2018), mucopolysaccharidosis type II (Hunter's disease) (Dufresne et al., 2017), traumatic brain injury (Mallah et al., 2018; Woods et al., 2013), Tay–Sachs/Sandhoff disease (Chen et al., 2008), and Niemann–Pick disease (Tobias, Pathmasiri, & Cologna, 2019) to name but a few. Indeed, MALDI-IMS was shown to be a powerful approach for probing amyloid plaque-associated lipid biochemistry in specific brain regions of transgenic AD mice models (Kaya, Zetterberg, et al., 2018). The widely used familial AD mouse model, 5xFAD, contains $Aβ_{42}$ peptide-rich amyloid plaque deposits in brain parenchyma (Oakley, Cole, & Logan, 2006). Further, the amyloid plaque-associated lipid biochemistry-related immune proteins have been extensively studied in 5xFAD mouse brain (Griciuc et al., 2019; Rangaraju et al., 2018; Ulland et al., 2017). Hence, lipid molecular information represents an important piece of the complex molecular puzzle in amyloid plaques and their interrelated discussion with amyloid plaque pathology might improve the understanding of amyloid-associated AD pathogenesis.

In this study, high-spatial resolution MALDI-IMS of coronal brain tissue sections of 12-month-old 5xFAD mice revealed focal amyloid plaque-associated depletion of several myelin-associated lipid species. Double staining of the consecutive sections with fluoromyelin and amyloid-specific antibodies revealed amyloid plaque-associated myelin lipid disruption which was specific to the edges of the corpus callosum in the white matter while there was no disruption of the myelin sheath observed in amyloid plaque-rich areas in several other brain regions in the gray matter. APOE accumulation in amyloid plaques was found to be in line with sulfatide depletion in several brain regions, suggesting that sulfatide depletion might be APOE deposition-associated in all the plaques in the white and gray matter regions in 5xFAD mouse brain. Our data suggests amyloid plaque pathology-associated disruption of the myelin sheath through the loss

of myelin lipids which leverages the understanding of gray matter and white matter pathologies in AD.

2 | MATERIALS AND METHODS

2.1 | Chemicals and reagents

All chemicals for matrix and solvent preparation were pro-analysis grade and obtained from Sigma-Aldrich (Stockholm) unless otherwise specified. Anti-beta amyloid antibody (rabbit polyclonal to beta amyloid), anti-APOE antibodies (rabbit monoclonal to apolipoprotein E) and thioflavin S, DAPI fluorescent stains were purchased from Abcam. FluoroMyelin™ green fluorescent myelin stain was purchased from ThermoFisher Scientific (Stockholm). TissueTek optimal cutting temperature (OCT) compound was purchased from Sakura Finetek (AJ Alphen aan den Rijn). The deionized H_2O was obtained from a Milli-Q purification system (Merck Millipore).

2.2 | Animals, tissue sampling and sectioning

The 5xFAD transgenic mouse model was purchased from Jackson Laboratory (Bar Harbor). These transgenic AD mice co-express five FAD mutations [APP K670N/M671L (Swedish) + I716V (Florida) + V717I (London) and PS1 M146L + L286V]. All mutations are specific to FAD and their expression is regulated under the control of the Thy-1 promoter to drive overexpression only in the brain. This exploratory animal study was not pre-registered. No randomization, blinding, and sample calculation was performed. No exclusion criteria were predetermined and no animals were excluded. All mice were obtained by breeding the 5xFAD mouse (Tg6799; The Jackson Laboratory) with B6SJLF1/J (The Jackson Laboratory). The animals were housed in individually ventilated cages and each cage housed 4–6 mice. All mice were kept at 20°C and 12-hr day/12-hr night cycle. Food and water were available ad libitum. Serial sections from the male 12-month-old transgenic (5xFAD) mice were used as the experimental group (n = 4) (mean weight: 23.4 g) and male non-transgenic littermates (LM) were used as the control animals (n = 4) (mean weight: 30.1 g). All animal procedures were approved by the Ethics Committee of the Animal Care and Use Committee of Acibadem Mehmet Ali Aydinlar University, Istanbul, Turkey (Approval ID: HDK-2016/13). The animals were anesthetized to minimize suffering with isoflurane and sacrificed by decapitation. The brains were dissected within 3 min postmortem delay and frozen on dry ice. Frozen tissue sections (10 μm thick) were cut in a cryostat microtome (Leica CM 1520; Leica Biosystems) at −20°C, and collected on indium tin oxide (ITO)-coated glass slides (Bruker Daltonics) and stored at −80°C. The control and transgenic mice brains were cut on the same ITO glasses (three sections for each) to avoid the effect of sample preparation variance during MALDI-IMS analysis. Immunohistochemistry and fluorescence staining experiments were performed on the direct consecutive tissue sections unless otherwise specified.

2.3 | Sample preparation and matrix application for MALDI-IMS

For MALDI-IMS in dual polarity, 1,5-diaminonapthalene matrix was deposited onto the tissue by sublimation-based matrix coating (Thomas, Charbonneau, Fournaise, & Chaurand, 2012). Matrix deposition for lipid analysis was carried out using a vacuum sublimation apparatus (Sigma-Aldrich) as previously described in detail elsewhere (Kaya, Jennische, Lange, & Malmberg, 2018a). 1,5-Diaminonapthalene matrix was deposited over the brain tissue sections with the optimized sublimation parameters: 20 min at a temperature of 130°C under a stable vacuum of ~0.8 mbar according to the previously published reports (Kaya, Michno, et al., 2017).

2.4 | MALDI-MS and MALDI-IMS and MALDI-MS/MS analyses

IMS analysis of tissue sections was performed on a MALDI-TOF/TOF UltrafleXtreme mass spectrometer equipped with a SmartBeam II Nd:YAG/355 nm laser operating at 1 kHz (Bruker Daltonics). MALDI-IMS data for lipids over a mass range of 300–3000 Da. was collected in reflective ion mode using 5–10 laser shots per pixel in negative polarity and 20–25 laser shots in positive polarity as previously described in detail elsewhere (Kaya, Michno, et al., 2017). External calibration was carried out using Peptide Calibration Standard I (Bruker Daltonics) solution (4 pmol/μl) spotted next to the tissue sections prior to sample preparation. Image data were reconstructed and visualized using Flex Imaging v3.0 (Bruker Daltonics). For Aβ peptide analyses on the brain tissue sections, spectral profiling data acquisitions were performed in linear positive ion mode by collecting 100 laser shot-spectra over a mass range of 2,000–10,000 Da. Identification of lipids and amyloid peptides (Aβ 1–40, Aβ 1–42) was performed by examining MS/MS spectra obtained in laser induced dissociation (LID)-TOF/TOF mode and comparing the diagnostic fragment ions from the LIPID MAPS database (Nature Lipidomics Gateway, www.lipidmaps.org) and previously published studies (Zemski Berry et al., 2011). LID-MALDI-TOF/TOF MS/MS spectra obtained from the precursor ions of lysophosphatidylcholine (LPC 16:0) (m/z 496.3), Cer(36:1 (m/z 564.6), and PE(36:1p) (m/z 728.5) along with the fragmentation pathways proposed for each molecule are provided as examples (Figure S1).

The localization of Aβ 1–40 and Aβ 1–42 in 5xFAD mouse brain has previously been shown on these samples (Kaya et al., 2019), with MALDI-MS and MALDI-IMS which are able to distinguish between the Aβ 1–40 and Aβ 1–42 in AD brain tissues (Carlred et al., 2016; Stoeckli, Staab, Staufenbiel, Wiederhold, & Signor, 2002). Here we focus solely on the lipid changes associated with the plaques and instead correlate the MALDI-IMS with immunohistochemical staining of the plaques.

Quantitative analysis of MALDI-MSI data is notoriously difficult. So as not to imply quantitation with the inclusion of numerical statistics the robustness and reproducibility of the results are demonstrated by the inclusion of multiple images from multiple 5xFAD and littermate control mice (Figures S6, S7).

2.5 | Immunohistochemistry, fluorescence staining, and hematoxylin staining

In order to visualize amyloid aggregates, the tissue sections were fixed in methanol, blocked with 2.5% horse serum and incubated with a rabbit polyclonal antibody against β-amyloid (ab2539; Abcam) diluted 1:2000 in phosphate-buffered saline (PBS), overnight. Impress reagent, anti-rabbit Ig (Vector Laboratories) was used as secondary reagent and the reaction was visualized using Liquid DAB + substrate chromogen system (DAKO). Nuclei were counterstained with hematoxylin and the sections were dehydrated and mounted in DPX (Merck). The sections were scanned using a slide scanner (NanoZoomer SQ; Hamamatsu Photonics). For myelin and amyloid double staining, the sections were fixed in 4% buffered formaldehyde for 5 min, rinsed in PBS and incubated with a rabbit polyclonal antibody against β-amyloid (ab2539; Abcam) diluted 1:1,000 in PBS, overnight. A Cy3 conjugated donkey anti-rabbit IgG diluted 1:300 in PBS, was used as the secondary reagent (Jackson laboratories 711-166-152). After rinsing, the sections were incubated for 20 min with FluoroMyelin™ green fluorescent myelin stain (F34651; Molecular Probes) diluted 1:300 in PBS. Nuclei were stained with bisbenzimide (33342; Hoechst) trihydrochloride (14533; Sigma Aldrich) diluted to 2.5 μg/ml in distilled water. The sections were mounted in Vectashield (Vector laboratories) and viewed with a Zeiss Axio Imager M1 microscope using the appropriate filter combinations. For APOE and amyloid double staining, the sections were fixed in methanol, air dried, and incubated with a rabbit monoclonal antibody against Apolipoprotein E (ab19378; Abcam) diluted 1:1,000 in PBS, overnight. Cy3 conjugated donkey anti-rabbit IgG was used as the secondary reagent (711-166-152; Jackson Laboratories) diluted 1:300 in PBS. After rinsing the sections were incubated with Thioflavin S (T1892; Sigma) 2mg/ml in PBS for 20 min. The sections were mounted in Vectashield (Vector Laboratories) and viewed with a Zeiss Axio Imager M1 microscope using the appropriate filter combinations. For general histology, the sections were fixed in methanol, immersed in Harris hematoxylin (Histolab Products AB) for 45 s, rinsed in water and immersed in 0.2% eosin in ethanol (Histolab Products AB) for 30 s. The sections were then dehydrated and mounted in DPX (Merck).

3 | RESULTS

3.1 | Myelin lipids are depleted in amyloid plaques in the hippocampus, cortex and on the edges of corpus callosum

Initially, chromogenic staining of amyloid plaques with anti-beta amyloid antibody and hematoxylin staining was performed on a coronal tissue section to reveal the plaque distributions over the brain regions in 12-month-old 5xFAD mice brains. Amyloid plaques were visualized abundantly in the cornu ammonis (CA), subiculum and deep cortical layers (Figure S2). For the inspection of the amyloid plaque-associated alterations of myelin lipids, regions containing both white matter and gray matter areas including the cortex, corpus callosum, and CA region in the hippocampus in coronal sections of 12-month-old 5xFAD mice brains were imaged using MALDI-IMS at 10 μm spatial resolution in negative and positive polarities (Figures 1 and 2). Further, consecutive tissue sections were stained with an anti-Aβ antibody and hematoxylin to distinguish amyloid plaques and brain regions, respectively (Figures 1a and 2a,m). Inspection of the ion images (in green) obtained in negative polarity analysis revealed significant focal depletion of both hydroxylated and non-hydroxylated sulfatides (ST), irrespective of their fatty acid (FA) moiety (Figure 1b–g), along with galactosylceramides (GalCer) (Figure 1h–j) and some plasmalogen phosphatidylethanolamines (PEp) (Figure 1k,l) in the hippocampal and cortical amyloid plaques in a coronal tissue sections of 12-month-old 5xFAD mice brain (Figure 1a). Inspection of the ion images (in green) obtained in positive polarity analysis revealed relatively less clear depletion of phosphatidylcholines (PC) (abundant in the myelin-rich corpus callosum) on the edges of the corpus callosum, whereas no clear depletion of these species was observed in the amyloid plaques in the cortex and CA regions in the gray matter (Figure 2b–d). PC species that were most abundant in the gray matter revealed no clear depletion in amyloid plaques in the gray or white matter (Figure 2e,f). Furthermore, LPCs (Figure 2g,h) and lysophosphatidylethanolamines (LPEs) (Figure 2p,q) were found to be accumulated in amyloid plaque areas in line with the depletion of certain PCs (Figure 2i–l) and PEps (Figure 2r). MALDI-IMS analysis of a different brain region containing the subiculum, CA and adjacent cortical areas revealed that ceramides, which are the possible precursor/degradation products of sulfatides, were found to be accumulated in amyloid plaques, particularly in the subiculum and adjacent CA region in line with the severe depletion of sulfatides (Figure 3). Chromogenic amyloid-specific immunostaining did not reveal any plaque-like accumulations in the brains of age-matched littermate control mice brain. Further, MALDI-IMS revealed distributions of the lipid species in the age-matched littermate control mice brain and there were no plaque-like accumulations/depletions of the same lipid species in the equivalent brain regions where plaque-associated lipid changes were observed in 12-month-old 5xFAD mice brain (Figure S3, S4). In addition, to increase the confidence in observations, MALDI-IMS of lipids and immunofluorescence amyloid staining of the same coronal tissue section of 5xFAD mice brain was performed which demonstrated localization of amyloid plaques and associated lipid alterations (Figure S5).

Ion images (obtained with MALDI-IMS in positive and negative polarities at 10 μm per pixel spatial resolution) of STs, GalCers, PEps, PCs, LPEs and LPCs from the coronal brain tissue sections of three 12-month-old 5xFAD mice are provided in Figure S6 and S7.

3.2 | Myelin structure is disrupted in the edges of corpus callosum in the white matter

While ion images of the aforementioned STs, GalCers, Peps, and certain PCs indicate their clear abundance in the myelin-rich corpus callosum (Figure 1) in the white matter and their depletion in amyloid plaques, it is not certain if the amyloid plaque-associated myelin lipid

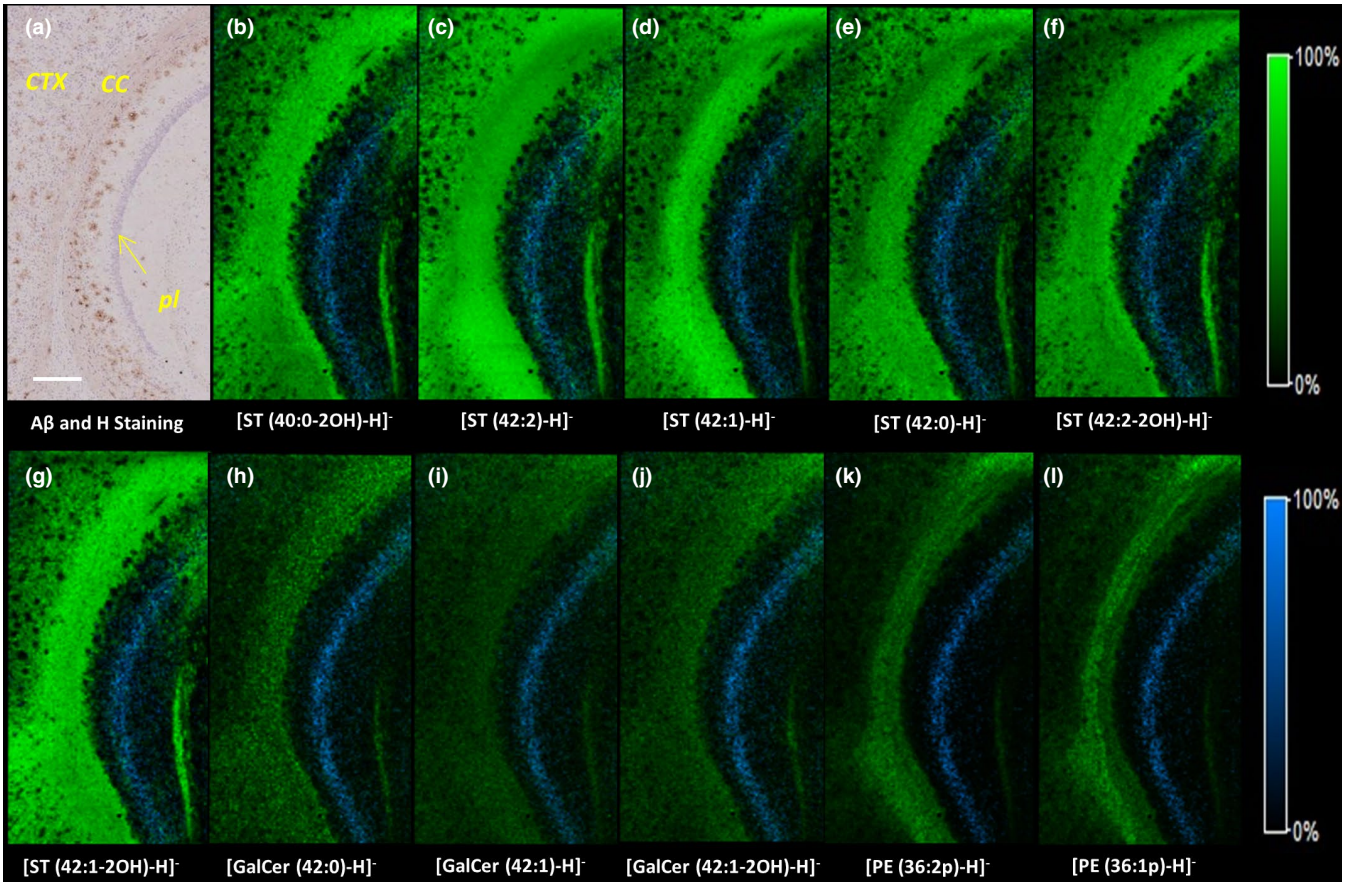

FIGURE 1 Matrix-assisted laser desorption/ionization imaging mass spectrometry (MALDI-IMS) reveals focal depletion of myelin lipids in amyloid plaques in the hippocampus, cortex and on the edges of corpus callosum in coronal brain tissue sections of 12-month old 5xFAD mouse (n = 4 mice, n = 3 sections each). (a) The spatial distribution of amyloid aggregates (brown aggregates) in the hippocampus and adjacent cortical regions was visualized with anti-beta amyloid antibody and counter staining with hematoxylin (CC: corpus callosum, CTX: cortex, pl: pyramidal layer). Significant depletion of several hydroxylated and non-hydroxylated sulfatides; (b) ST(40:0-2OH) (m/z 878.6), (c) ST(42:2) (m/z 888.6), (d) ST(42:1) (m/z 890.6), (e) ST(42:0) (m/z 892.6), (f) ST(42:2-2OH) (m/z 904.6), (g) ST(42:2-2OH) (m/z 906.6), irrespective of their fatty acid moiety, along with the depletion of some galactosylceramides; (h) (GalCer) (42:0) (m/z 812.3), (i) GalCer(42:1) (m/z 810.3), (j) GalCer(42:1-2OH) (m/z 848.3) and plasmalogen phosphatidylethanolamines; (k) PE(36:2p) (m/z 726.5), (l) PE(36:1p) (m/z 728.5) in amyloid plaques in the hippocampus, cortex and on the edges of corpus callosum. Ion images of putatively assigned lysophosphatidylethanolamine (LPE) (13:0) (m/z 410.3) in blue were overlayed to highlight pyramidal cell layers in panels (b–l) for clearer visualization of the data and comparison with the stained image in (a). MALDI-IMS analysis was performed at 10 μm per pixel spatial resolution in negative ion mode. Ions are either $[M + H]^+$ or $[M–H]^-$ unless otherwise specified otherwise. Scale bar in panel (A) is 200 μm

loss is correlated with structural disruption of the lipid-reach myelin sheath in 5xFAD mouse brain. Since myelin is a particularly lipid-reach brain region; one would expect plaque-associated structural deformation of the myelin sheath due to the lipid loss. Therefore, consecutive coronal tissue sections were double stained with fluoromyelin fluorescence and anti-amyloid immunofluorescence (Figure 4a–c). This revealed clear amyloid plaque-associated myelin disruption but only on the edges of the corpus callosum in the white matter (Figure 4d–f). The myelin structure was not disrupted in amyloid plaque areas in several other brain regions including the cortex (Figure 5a–c), dentate gyrus (Figure 5d–f), CA (Figure 5g–l), and subiculum (Figure 5j–l) in the gray matter. This suggests amyloid plaque-associated disruption of the lipid reach myelin sheath which links amyloid pathology to white matter lipid degeneration. Results from three more 12-month-old 5xFAD mice brains are presented in Figure S8.

3.3 | APOE is present in amyloid plaques in the gray matter and on the edges of corpus callosum

APOE is synthesized and secreted primarily by astrocytes and microglia in the CNS (Boyles, Pitas, Wilson, Mahley, & Taylor, 1985; Nakai, Kawamata, Taniguchi, Maeda, & Tanaka, 1996). As mentioned above, it has been postulated that APOE mediates sulfatide depletion in APP transgenic mice models using shot gun lipidomic analysis of brain tissue extracts (Cheng et al., 2010). It has also been reported that the densities of astrocytes (glial fibrillary acidic protein) and microglia (F4/80) implicated in neuroinflammation are increased in/around $A\beta_{42}$-rich amyloid plaques in aged 5xFAD mouse brain (Oakley et al., 2006) which suggests a possible route for accumulation of APOE in/around amyloid plaques. Therefore, to test if APOE is accumulated and can be correlated with severe sulfatide depletion in amyloid plaques in

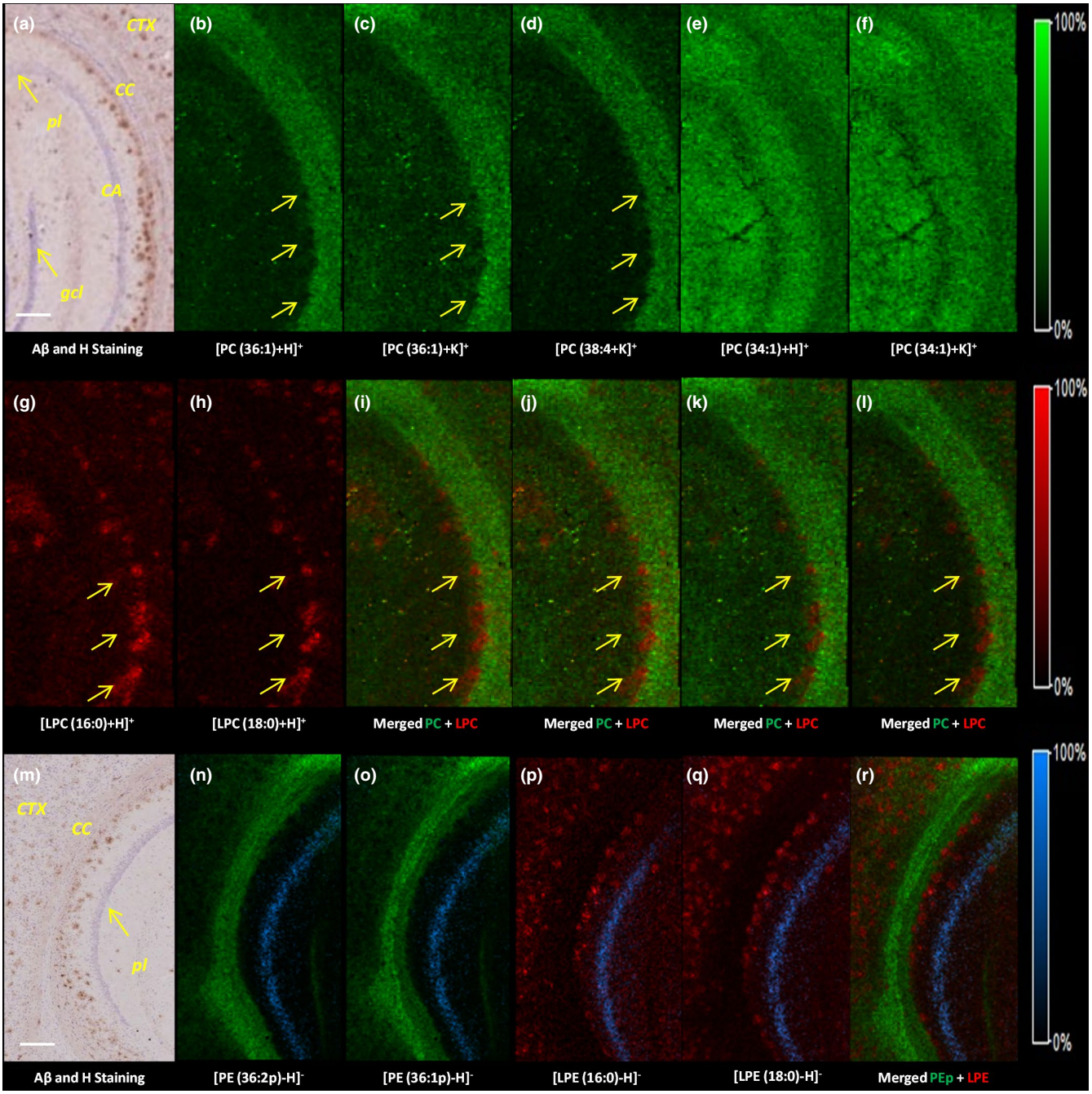

FIGURE 2 Matrix-assisted laser desorption/ionization imaging mass spectrometry (MALDI-IMS) reveals focal depletion of certain phosphatidylcholines (PCs) that are abundant in myelin-rich corpus callosum are depleted in amyloid plaques on the edges of the corpus callosum (see yellow arrows in panel (b–d) for the depletion areas) (n = 4 mice, n = 3 sections each). Lysophosphatidycholines (LPCs) are accumulated in amyloid plaques in the whiter matter and grey matter. Accumulations of lysophosphatidylethanolamines were observed in the amyloid plaques where plasmalogen phosphatidylethanolamines are depleted. (a, m) Spatial distribution of amyloid aggregates (brown aggregates) in the hippocampus and adjacent cortical regions was visualized with anti-beta amyloid antibody and counter staining with hematoxylin. Ion images of phosphatidylcholines (b) PC(36:1) (m/z 788.6), (c) PC(36:1)+K (m/z 826.6), (d) PC(38:4)+K (m/z 848.6), (e) PC(34:1) (m/z 760.6), (f) PC(34:1)+K (m/z 798.6), (g) LPC(16:0) (m/z 496.3), (h) LPC(18:0) (m/z 524.3), (i) merged PC(36:1) (m/z 788.6) (green), LPC(16:0) (m/z 496.3) (red), (j) merged) PC(36:1)+K (m/z 826.6) (green), LPC(16:0) (m/z 496.3) (red), (k) PC(38:4)+K (m/z 848.6) (green) and LPC(16:0) (m/z 496.3) (red), (l) PC(38:4)+K (m/z 848.6) (green) and LPC(18:0) (m/z 524.3) (red), (n) PE(36:2p) (m/z 726.5). Imaging of phosphatidylethanolamines (o) PE(36:1p) (728.5), (p) lysophosphatidylethanolamine (LPE) (16:0) (m/z 452.5), (q) LPE(18:0) (m/z 480.5), (r) merged PE(36:1p) (728.5) (green) and LPE(18:0) (m/z 480.5) (red). Ion images of putatively assigned LPE(13:0) (m/z 410.3) in blue were overlayed to highlight pyramidal cell layers in panels (n–r) for better visualization of the data. MALDI-IMS analysis was performed at 10 μm per pixel spatial resolution in positive (b–l) and negative (n–r) ion modes. Ions are either $[M + H]^+$ or $[M–H]^-$ unless otherwise specified otherwise.CC, corpus callosum; CTX, cortex; CA, cornu ammonis; pl, pyramidal layer; gcl, granular cell layer. Scale bars, panels (a, m), 200 μm

the gray matter and on the edges of the corpus callosum in 12-month-old 5xFAD mouse brain (Figure 1), coronal brain tissue sections were double stained with thioflavin S and monoclonal anti-APOE antibody (Figure 6). The results showed accumulation of APOE protein in all the amyloid plaques in the gray matter and on the edge of the corpus callosum supporting the hypothesis of an association of APOE with sulfatide depletion in the amyloid plaques in 12-month-old 5xFAD mouse brain. Results from three other 12-month-old 5xFAD mice brains are presented in Figure S9.

4 | DISCUSSION

The myelin sheath is a lipid rich, multilamellar extension of the plasma membrane of oligodendrocytes. In contrast to most biological membranes, myelin contains remarkably high lipid levels which account for 70%–85% of its dry weight (Wang, Palavicini, & Han, 2018). Lipidomics studies have revealed that galactosylceramide and their sulfated form, sulfatides, are the most typical lipids of myelin, where they are highly enriched and their abundance was found to be proportional to the amount of myelin present in the rat brain (Norton & Poduslo, 1973). In addition to galactolipids, cholesterol, ethanolamine-containing plasmalogens, phosphatidylethanolamines, phosphatidycholines and sphingomyelin are also major lipid constituents of the myelin sheath (Norton & Poduslo, 1973) (Wang et al., 2018).

This study reports the loss of myelin-associated lipids, disruption of myelin sheath, and APOE deposition localized to amyloid plaques in aged (12-month-old) 5xFAD mouse brain tissue. The goal was to shed further light on the molecular, morphological, and immune signatures of myelin lipid loss in association with amyloid pathology in AD in a spatially specific manner. Amyloid plaques are exceedingly rare in the white matter in AD pathology (Nasrabady et al., 2018). This is apparent here with 12 month-old 5xFAD mouse brain in which we observed amyloid plaque accumulations abundantly in the gray matter areas including subiculum, cortex, CA and DG, while there were a few plaques visible on the edges of corpus callosum in the white matter (Figure S2b). The presence of the latter results in a direct exposure of myelin-rich corpus callosum in the white matter to amyloid plaques rich in Aβ 1–42 and Aβ 1–40 (Oakley et al., 2006).

It was previously demonstrated that Aβ peptides, particularly Aβ 1–42, are toxic to oligodendrocytes and can lead to their increased apoptotic cell death (Desai et al., 2010; Xu et al., 2001). The abundant lipid structural components of the myelin sheath, sulfatides, are mainly found in oligodendrocytes (the myelinating cells) in the CNS (Hirahara et al., 2017), whereas low amounts have been detected in neurons and astrocytes (Isaac et al., 2006). Therefore, it can be inferred that Aβ-induced degeneration of oligodendrocytes might lead to severe loss of myelin lipids, particularly sulfatides, which can cause degeneration of the myelin sheath in amyloid plaques on the edges of the corpus callosum as observed here. Shotgun lipidomic analysis of brain tissue extracts has previously revealed that decreases in sulfatide levels coincide with the elevation of ceramides in early stages of AD (Han et al., 2002). Here, MALDI-IMS reveals co-localization of the accumulation of ceramides and the depletion of sulfatides in amyloid plaques in several brain regions including cortex, subiculum and CA and on the edges of corpus callosum in the 5xFAD mouse brain (Figure 3). While ceramides may arise as possible precursor/degradation products of sulfatides, a body of evidence suggests that the ceramide elevation results from Aβ-mediated activation of sphingomyelinases (SMases) that catalyze the breakdown of sphingomyelins (SMs) to ceramides (Jana & Pahan, 2004; Lee et al., 2004). Grimm et al. reported increased activity of SMases in presenilin-FAD mutations (that also exist in 5xFAD), where Aβ1-42 directly activates neutral SMase (Grimm et al., 2005). In our imaging analysis, no clear changes in sphingomyelin levels in amyloid plaques were observed in 12 month old 5xFAD mouse brain (data not shown).

The mechanism of sulfatide depletion in amyloid plaques still remains elusive. The content of sulfatides in the CNS is modulated by APOE protein in an isoform-dependent manner through APOE-containing CNS lipoproteins (Han et al., 2003). APOE, the lipid transport protein expressed by microglia (Nakai et al., 1996) and astrocytes (Boyles et al., 1985) in the brain was also evidenced to be essential for Aβ deposition in APP^{V717F} AD mouse model (Bales et al., 1999). To identify the mechanisms of sulfatide depletion in AD, Han et al. (Han, 2007) proposed a working mechanism which suggests APOE-associated lipoprotein particles released from astrocytes can acquire sulfatides from the myelin sheath through a ''kiss-and-run'' mechanism. This is then followed by metabolism and degradation of the resulting sulfatide-containing APOE-associated lipoprotein particles through endocytic pathways. This hypothesis was tested by Cheng et al. (Cheng et al., 2010) using two human APP expressing tg mice, PD (APP_{V71F}) and tg2576 ($APP_{Swe\ 670/671}$), both of which display extensive amyloid plaques. Analysis by shotgun lipidomics was used to demonstrate that the sulfatide levels were reduced in both animals in an Aβ pathology-dependent and age-dependent manner and sulfatide depletion did not occur in APP mutant, APOE null ($APOE^{-/-}$) animals relative to the $APOE^{-/-}$ controls. This provides evidence for the association of APOE with sulfatide depletion in AD pathogenesis (Cheng et al., 2010). Further, the brains of APP tg mice, tg2576 ($APP_{Swe\ 670/671}$), and indeed 5xFAD (Hong et al., 2013) have higher APOE levels relative to age-matched controls. Accumulation of astrocytes (glial fibrillary acidic protein) and microglia (F4/80) as a response to amyloid pathology in 5xFAD mouse brain (Oakley et al., 2006) suggests a possible route for accumulation of APOE in/around amyloid plaques. In our study, we imaged the APOE distribution and observed clear deposition of APOE in/around the amyloid plaques in the gray and white matter in 12-month-old 5xFAD mouse brain (Figure 6). This is in line with the severe depletion of several sulfatide species in all the amyloid plaques in the grey matter and white matter (Figure 1). Thus, it can be hypothesized that the elevated levels of APOE, a result of the immune response to amyloid deposition, irrespective of the brain region, can facilitate the depletion of sulfatides through APOE-associated lipoprotein metabolism in/around Aβ plaques.

FIGURE 3 Matrix-assisted laser desorption/ionization imaging mass spectrometry (MALDI-IMS) reveals colocalized depletions of sulfatides and elevations of long-chain ceramides in amyloid plaques in the cortex, and hippocampus in 12-month old 5xFAD mouse brain (n = 4 mice, n = 3 sections each). (a) Spatial distribution of amyloid aggregates (brown aggregates) in the hippocampus and adjacent cortical regions in 12-month-old 5xFAD mouse brain visualized with anti-beta amyloid antibody and counterstaining with hematoxylin. Ion images of sulfatides, (b) ST(36:1) (m/z 806.6), (c) ST(40:1) (m/z 862.6), (d) ST(40:2-2OH) (m/z 878.6), (e) ST(42:2) (m/z 888.6), (f) ST(42:1) (m/z 890.6), (g) ST(42:2-2OH) (m/z 904.6), (h) ST(42:1-2OH) (m/z 906.6) reveals their clear depletion in amyloid plaques while ion images of ceramides, (i) (Cer(36:1) (m/z 564.6), (j) CerP (42:1) (m/z 648.6) show accumulation in amyloid plaques. Exemplified merged ion images of sulfatides and ceramides, (k) ST(36:1) (m/z 806.6) and (Cer(36:1) (m/z 564.6), (l) ST(42:2) (m/z 888.6) and (Cer(36:1) (m/z 564.6), (m) ST(42:1) (m/z 890.6) and (Cer(36:1) (m/z 564.6), (n) ST(42:2) (m/z 888.6) and CerP (42:1) (m/z 648.6), (o) ST(42:1) (m/z 890.6) and CerP (42:1) (m/z 648.6) reveals the clear colocalization of the depletion of sulfatides and accumulation of ceramides in amyloid plaques in 12-month-old 5xFAD mouse brain. Ion images of putatively assigned lysophosphatidylethanolamine (LPE) (13:0) (m/z 410.3) in blue were overlayed to highlight pyramidal cell layers in panels (b–o) for better visualization of the data. MALDI-IMS analysis was performed at 10 μm per pixel spatial resolution in negative ion mode. Ions are either $[M + H]^+$ or $[M-H]^-$ unless otherwise specified otherwise. CC, corpus callosum; CTX, cortex; CA, cornu ammonis; SUB, subiculum; pl, pyramidal layer; gcl, granular cell layer. Scale bars, panels (a, m), 200 μm

Significant depletion of ethanolamine plasmalogen phospholipids has been reported in human AD subjects and transgenic AD mice models (Ginsberg, Rafique, Xuereb, Rapoport, & Gershfeld, 1995; Han et al., 2001b; Igarashi et al., 2011) and this depletion is AD specific compared to the primary site of neurodegeneration in either Huntington's disease (caudate nucleus) or Parkinson's disease (substantia nigra) (Ginsberg et al., 1995). PC species were also reported to be diminished in AD subjects (Whiley et al., 2014). Oxidative stress (Farooqui, Rapoport, & Horrocks, 1997), inflammation (Katafuchi et al., 2012), and peroxisome dysfunction (Kou et al., 2011) are possible amyloid plaque-associated mechanisms that have been proposed for plasmalogen depletion in AD. Indeed, Aβ peptide deposits, damaged neurons, and glial cells are obvious stimuli for focal inflammation in AD due to their discrete, localized accumulation (Akiyama et al., 2000; Heneka et al., 2015). Amyloid peptides and inflammatory mediators accumulated in amyloid plaques can upregulate the activity of PLA_2 enzymes which can result in the depletion of plasmalogen PEs and phosphatidylcholines in amyloid plaques. Indeed, partial accumulation of PLA_2 around Aβ plaques has been shown by immunostaining in 5xFAD mouse brain, which suggests a stimulated activity of this enzyme and underlies focal amyloid-associated inflammatory processes (Hong et al., 2016). Here, accumulations of LPE and LPC species in amyloid plaques (Figure 3) suggest a mechanism involving inflammatory activation of PLA_2 in association with amyloid plaques. On the other hand, plaque-associated oxidative stress can result in degradation of plasmalogens by reactive oxygen species (ROS). Plasmalogens are particularly susceptible to oxidative stress due to a vinyl-ether group in their molecular structure and may act as scavengers to protect lipids and lipoproteins from oxidative damage (Su, Wang, & Sinclair, 2019). Therefore, depletion of plasmalogens can exacerbate the focal oxidative damage to the lipids and proteins in amyloid plaques in 5xFAD mice brains. Additionally, increased levels of Aβ-induced ROS can also induce peroxisomal dysfunction, thus reducing alkyl-dihdroxyacetone phosphate synthase (AGPS) protein stability, which in turn decreases PE-PL synthesis, due to the dysfunction in peroxisomes where plasmalogens are biosynthesized (Grimm et al., 2011).

Upregulation of LPC species in amyloid plaques can be also implicated in focal demyelination (Mitew et al., 2010). LPC induces focal demyelination (Allt, Ghabriel, & Sikri, 1988; Hall, 1972) and disrupts myelin lipids nonspecifically (Plemel et al., 2018). This is in line with the myelin lipid loss in amyloid plaques, particularly in the myelin lipid-rich corpus callosum, in aged 5xFAD mouse brain (Figure 3), which might suggest a role of LPC for the disruption of the lipid-rich myelin sheath in this region.

Additionally, depletion of myelin lipids in amyloid plaques can be involved in the discussion of well-studied lipid metabolism-related amyloid plaque immunity in 5xFAD mouse brain such as the studies on the microglial receptor, triggering receptor expressed on myeloid cells 2 (TREM2). TREM2 lipid sensing was shown to sustain microglial response and metabolic fitness around the amyloid plaques and limits the diffusion and toxicity of amyloid plaques (Wang et al., 2016) in 5xFAD mice brain. Human TREM2 reporter cells were found to be stimulated by various phospholipids and non-phosphate anionic and zwitterionic lipids including sulfatides (Ulland et al., 2017; Wang et al., 2015). Further, elevated TREM2 expression in microglia by elevated TREM2 gene dosage in 5xFAD mice reshapes microglial response which ameliorates AD neuropathology (Lee et al., 2018). Therefore, it might be hypothesized that significant focal loss of anionic sulfatides and plasmalogen PEs might impair TREM2 lipid sensing, particularly in the myelin lipid-rich corpus callosum, and limit the microglial activation for degradation of Aβ in 5xFAD mice brain.

Taken together, high-spatial resolution MALDI-IMS of coronal brain tissue sections of 12-month-old 5xFAD mouse revealed focal amyloid plaque-associated depletion of several myelin-associated lipid species. Double staining of the consecutive sections with fluoromyelin and amyloid-specific antibody revealed amyloid plaque-associated myelin lipid disruption which occurs specifically on the edges of the corpus callosum in the white matter while there was no disruption of myelin sheath observed in amyloid plaque areas in several other brain regions in the grey matter. APOE accumulation in amyloid plaques is in line with sulfatide depletion in several brain regions suggesting that sulfatide depletion might be APOE deposition associated as an immune response to amyloid aggregation in all the plaques in the white and grey matters in 5xFAD mouse brain. Our data leverage the understanding of morphological, molecular, and immune signatures of amyloid plaque-associated myelin lipid loss in a brain region-specific manner. It is particularly

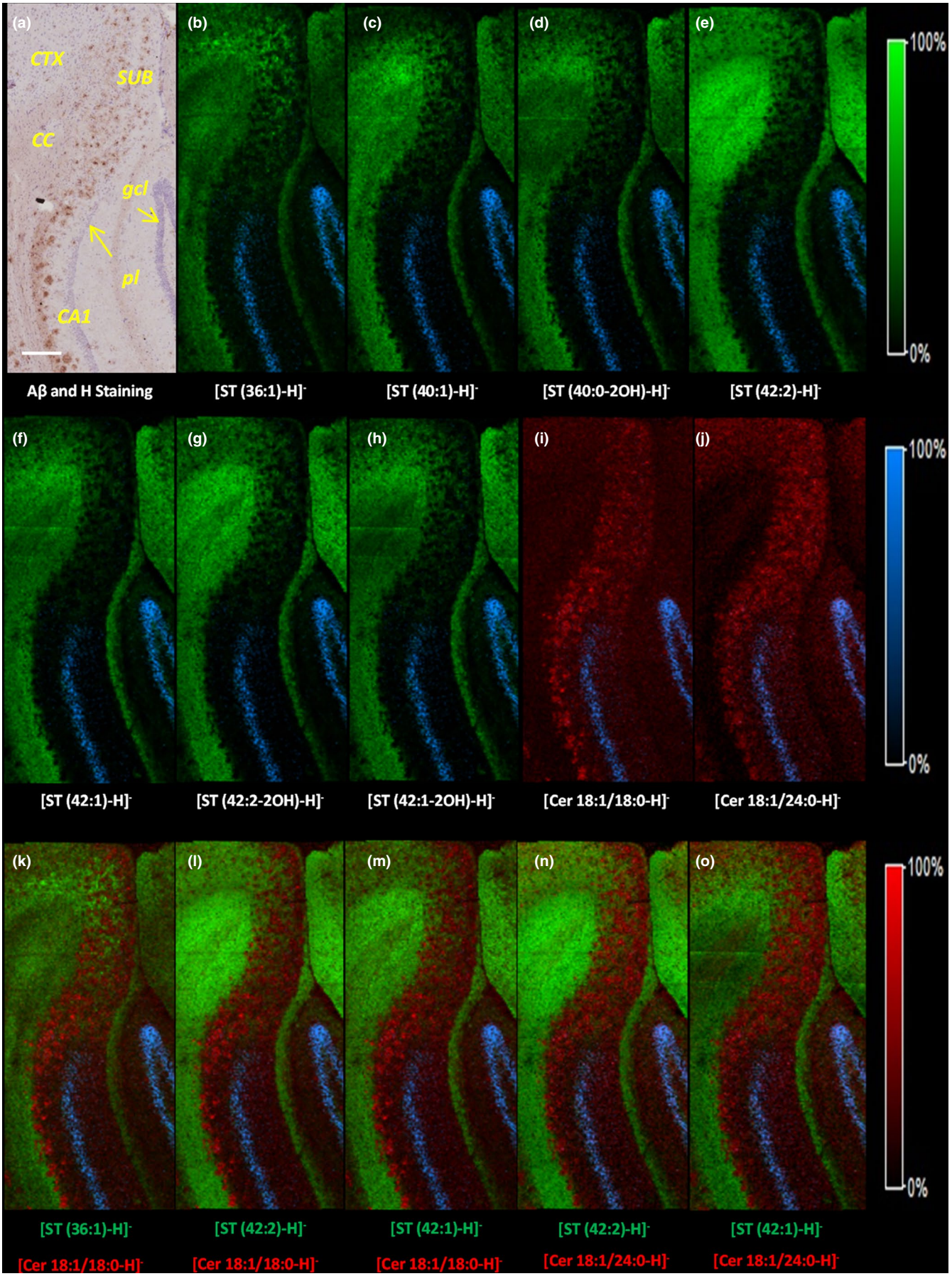
(a)
CTX
SUB
CC
gcl
pl
CA1
Aβ and H Staining
(b)
[ST (36:1)-H]-
(c)
[ST (40:1)-H]-
(d)
[ST (40:0-2OH)-H]-
(e)
[ST (42:2)-H]-
100%
0%
(f)
[ST (42:1)-H]-
(g)
[ST (42:2-2OH)-H]-
(h)
[ST (42:1-2OH)-H]-
(i)
[Cer 18:1/18:0-H]-
(j)
[Cer 18:1/24:0-H]-
100%
0%
(k)
[ST (36:1)-H]-
[Cer 18:1/18:0-H]-
(l)
[ST (42:2)-H]-
[Cer 18:1/18:0-H]-
(m)
[ST (42:1)-H]-
[Cer 18:1/18:0-H]-
(n)
[ST (42:2)-H]-
[Cer 18:1/24:0-H]-
(o)
[ST (42:1)-H]-
[Cer 18:1/24:0-H]-
100%
0%

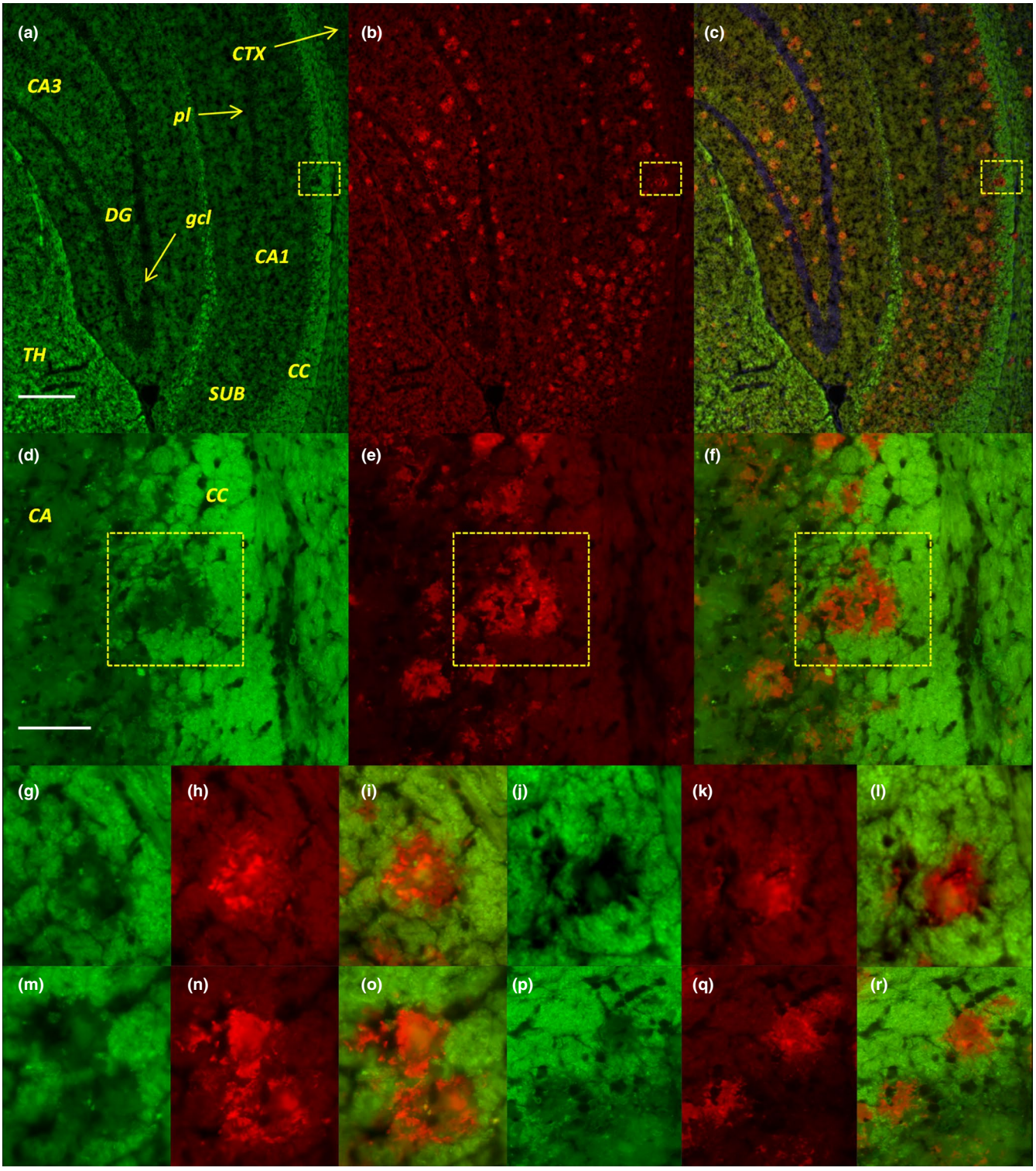

FIGURE 4 Double staining of coronal brain tissue sections with FluoroMyelin (in green), and anti-amyloid beta (Aβ) antibody (in red) reveals focal amyloid plaque-associated disruption of myelin on the edge of corpus callosum in the white matter of 12-month-old 5xFAD mice brain (n = 4 mice, n = 3 sections each). Coronal tissue sections were stained with (a) FluoroMyelin (in green) and (b) anti-Aβ antibody (in red). Panel (c) shows the merged images of FluoroMyelin (in green), anti-Aβ antibody (in red) and Hoechst staining (in blue). Panels (d–f) contain the zoomed images from the dashed squares in panels (a–c) showing the disruption of the myelin sheath (d), the amyloid plaque (e) and an overlay of these images (f) in the corpus callosum. Further examples of the disrupted myelin sheath in the amyloid plaques on the edges of corpus callosum are shown in panels (g–i), (j–l), (m–o), and (p–r). Hipp, Hippocampus; CA, cornu ammonis; CC, corpus callosum; CTX, cortex; TH, Thalamus; DG, dentate gyrus; Hipp, hippocampus; pl, pyramidal layer; gcl, granule cell layer. Original magnification, panel (a–c) ×10, and panel (d–r) ×40. Scale bars in panel (a, d) are 200 μm

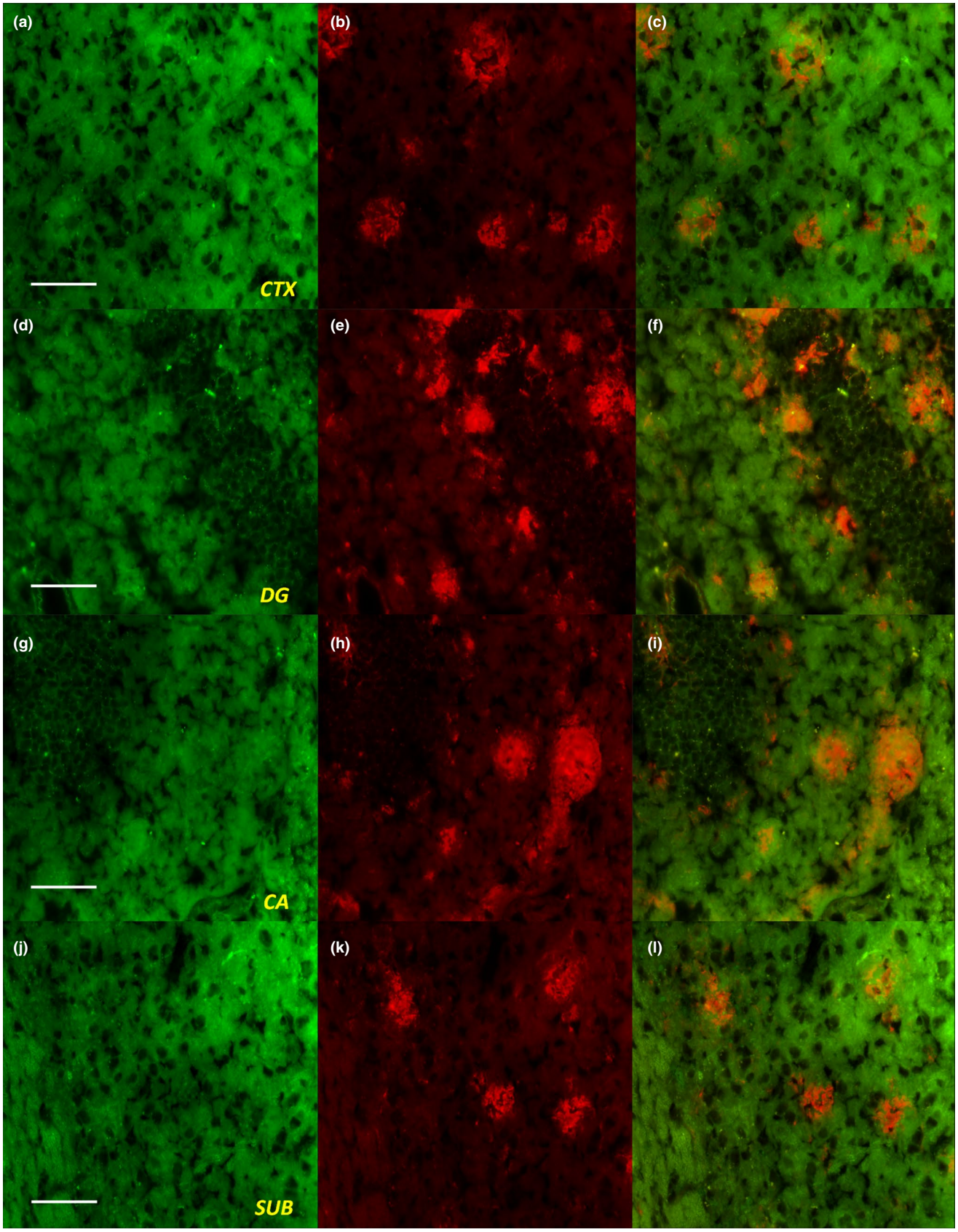

FIGURE 5 Double staining of coronal brain tissue sections with (a, d, g, j) FluoroMyelin (in green), and (b, e, h, k) anti-amyloid beta (Aβ) antibody (in red) shows no evidence of focal amyloid plaque-associated disruption of myelin in the (a–c) cortex (CTX), (d–f) dentate gyrus (DG), (g–i) cornu ammonis (CA), and (j–l) subiculum (SUB) in 12-month-old 5xFAD mice brain (n = 4 mice, n = 3 sections each). Panel (c, f, i, l) indicates merged images of FluoroMyelin (in green), and anti-Aβ antibody (in red). Original magnification, panel (a–l) ×40. Scale bars in panel (a, d, g, j) are 200 μm

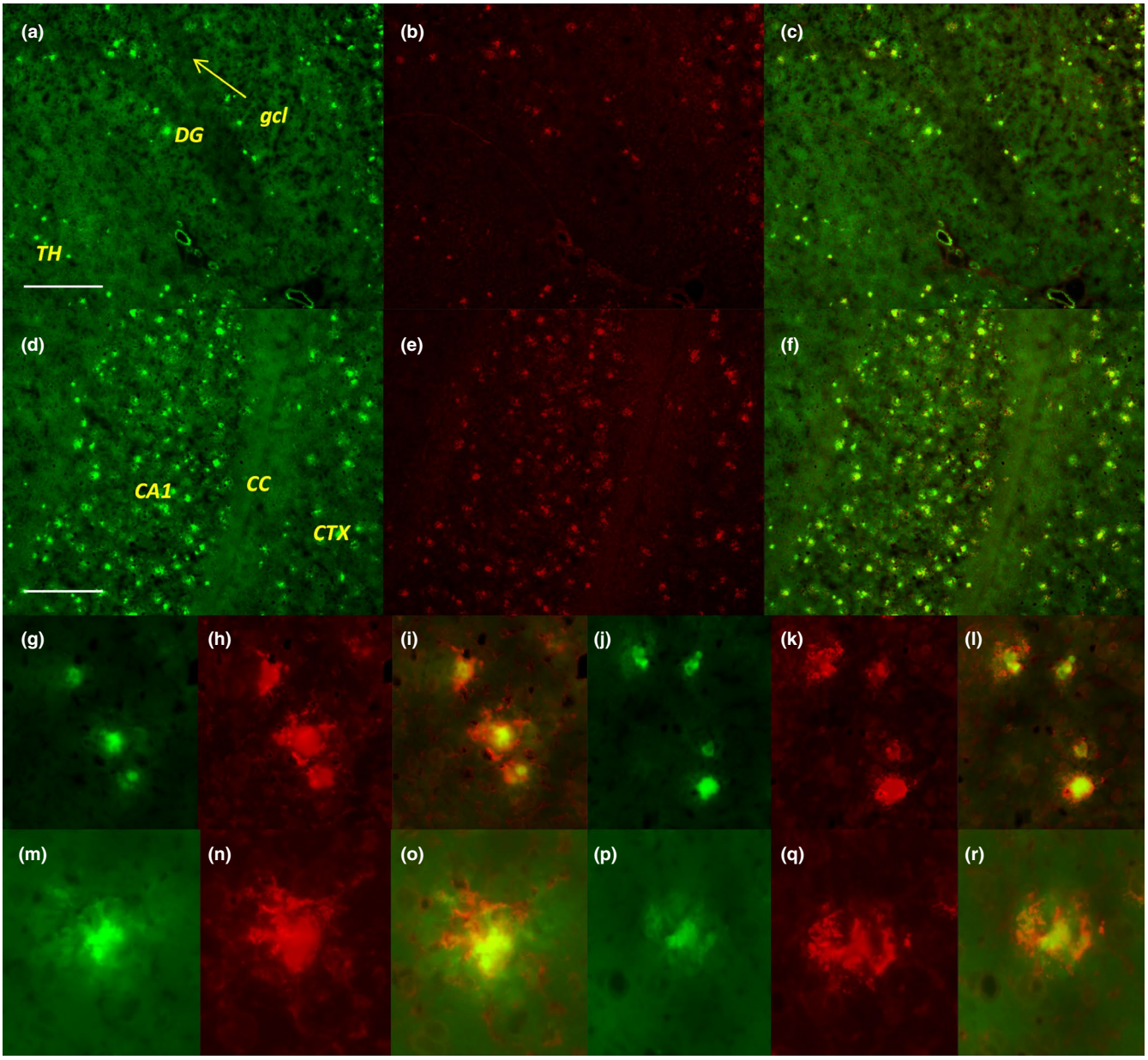

FIGURE 6 Double staining of coronal brain tissue sections with thioflavin S and anti-apolipoprotein E (APOE) antibody reveals accumulation of APOE in fibrillary amyloid plaques in several brain regions. (a, d) Thioflavin S and (b, e) APOE antibody stained brain regions including gray matter and white matter areas reveals (a–c), (d–f) colocalization of thioflavin S and APOE in the amyloid plaques in hippocampal and cortical brain regions including the edges of corpus callosum (CC). Zoomed image examples of colocalized thioflavin S and APOE in fibrillary amyloid plaques obtained from several brain regions (g–i) cornu ammonis (CA), (j–l) dentate gyrus (DG), (m–o) cortex (CTX), and (p–r) the edge of CC. TH: thalamus, gcl: granular cell layer, Original magnification, panels (a–f) ×10 and panels (g–r) ×40. Scale bars in panel (a, d) are 200 μm

important that our data suggest an amyloid-associated degradation of white matter through the disruption of myelin lipids and therefore provides a direct connection between the extracellular amyloid plaques and the degeneration of myelin in white matter.

ACKNOWLEDGMENTS

MALDI-IMS experiments were performed at the go:IMS imaging MS collaborative platform at the University of Gothenburg/Chalmers University of Technology (www.go-ims.gu.se). The authors thank Prof. Andrew G. Ewing for useful discussion; help with the preparation of the manuscript and generous support for the reagents used in this study. This study was financially supported by the LUA/ALF Agreement, Sahlgrenska University Hospital, the Swedish Research Council (VR), the Knut and Alice Wallenberg Foundation, the USA National Institutes of Health (NIH), European Research Council (ERC), The Scientific and Technological Research Council of Turkey (TUBITAK).

All experiments were conducted in compliance with the ARRIVE guidelines.

CONFLICT OF INTEREST

Authors declare no competing financial interest.

AUTHOR CONTRIBUTIONS

I.K. conceived the original idea. I.K., E.J., P.M., and J.S.F. designed the study. I.K. coordinated the study with the guidance of P.M., A.T.B., and J.S.F. I.K., E.J., S.L. designed and performed the classical histology and immunostaining experiments, analyzed, and interpreted the data. I.K. designed and performed the MALDI-IMS experiments, analyzed, and interpreted the data. All the authors discussed, commented, and interpreted the final data. A.T.B. and his laboratory maintained the mouse lines, selected and provided the brain tissue used for the studies presented here. I.K. generated the figures and wrote the manuscript and S.L., E.J., P.M., A.T.B., and J.S.F. critically reviewed it. All the authors approved the final version of the manuscript.

ORCID

Ibrahim Kaya https://orcid.org/0000-0003-3345-5602
Per Malmberg https://orcid.org/0000-0002-6487-7851
John S. Fletcher https://orcid.org/0000-0002-9418-8571

REFERENCES

Akiyama, H., Barger, S., Barnum, S., Bradt, B., Bauer, J., Cole, G. M., … Finch, C. E. (2000). Inflammation and Alzheimer's disease. *Neurobiology of Aging*, *21*, 383–421. https://doi.org/10.1016/S0197-4580(00)00124-X

Allt, G., Ghabriel, M., & Sikri, K. (1988). Lysophosphatidyl choline-induced demyelination. *Acta Neuropathologica*, *75*, 456–464. https://doi.org/10.1007/BF00687132

Bales, K. R., Verina, T., Cummins, D. J., Du, Y., Dodel, R. C., Saura, J., … Paul, S. M. (1999). Apolipoprotein E is essential for amyloid deposition in the APPV717F transgenic mouse model of Alzheimer's disease. *Proceedings of the National Academy of Sciences of the United States of America*, *96*, 15233–15238. https://doi.org/10.1073/pnas.96.26.15233

Bandaru, V. V. R., Troncoso, J., Wheeler, D., Pletnikova, O., Wang, J., Conant, K., & Haughey, N. J. (2009). ApoE4 disrupts sterol and sphingolipid metabolism in Alzheimer's but not normal brain. *Neurobiology of Aging*, *30*, 591–599. https://doi.org/10.1016/j.neurobiolaging.2007.07.024

Bartzokis, G. (2004). Age-related myelin breakdown: A developmental model of cognitive decline and Alzheimer's disease. *Neurobiology of Aging*, *25*, 5–18. https://doi.org/10.1016/j.neurobiolaging.2003.03.001

Behrendt, G., Baer, K., Buffo, A., Curtis, M. A., Faull, R. L., Rees, M. I., … Dimou, L. (2013). Dynamic changes in myelin aberrations and oligodendrocyte generation in chronic amyloidosis in mice and men. *Glia*, *61*, 273–286. https://doi.org/10.1002/glia.22432

Boyles, J. K., Pitas, R. E., Wilson, E., Mahley, R. W., & Taylor, J. (1985). Apolipoprotein E associated with astrocytic glia of the central nervous system and with nonmyelinating glia of the peripheral nervous system. *The Journal of Clinical Investigation*, *76*, 1501–1513. https://doi.org/10.1172/JCI112130

Bu, G. (2009). Apolipoprotein E and its receptors in Alzheimer's disease: Pathways, pathogenesis and therapy. *Nature Reviews Neuroscience*, *10*, 333. https://doi.org/10.1038/nrn2620

Carlred, L., Michno, W., Kaya, I., Sjövall, P., Syvänen, S., & Hanrieder, J. (2016). Probing amyloid-β pathology in transgenic Alzheimer's disease (tgArcSwe) mice using MALDI imaging mass spectrometry. *Journal of Neurochemistry*, *138*, 469–478. https://doi.org/10.1111/jnc.13645

Caughlin, S., Maheshwari, S., Agca, Y., Agca, C., Harris, A. J., Jurcic, K., … Whitehead, S. N. (2018). Membrane-lipid homeostasis in a prodromal rat model of Alzheimer's disease: Characteristic profiles in ganglioside distributions during aging detected using MALDI imaging mass spectrometry. *Biochimica Et Biophysica Acta (BBA) – General Subjects*, *1862*, 1327–1338. https://doi.org/10.1016/j.bbagen.2018.03.011

Chen, Y., Allegood, J., Liu, Y., Wang, E., Cachón-González, B., Cox, T. M., … Sullards, M. C. (2008). Imaging MALDI mass spectrometry using an oscillating capillary nebulizer matrix coating system and its application to analysis of lipids in brain from a mouse model of Tay^{-} Sachs/Sandhoff disease. *Analytical Chemistry*, *80*, 2780–2788. https://doi.org/10.1021/ac702350g

Cheng, H., Zhou, Y., Holtzman, D. M., & Han, X. (2010). Apolipoprotein E mediates sulfatide depletion in animal models of Alzheimer's disease. *Neurobiology of Aging*, *31*, 1188–1196. https://doi.org/10.1016/j.neurobiolaging.2008.07.020

Collins-Praino, L. E., Francis, Y. I., Griffith, E. Y., Wiegman, A. F., Urbach, J., Lawton, A., … Brickman, A. M. (2014). Soluble amyloid beta levels are elevated in the white matter of Alzheimer's patients, independent of cortical plaque severity. *Acta Neuropathologica Communications*, *2*, 83. https://doi.org/10.1186/s40478-014-0083-0

Corder, E. H., Saunders, A. M., Strittmatter, W. J., Schmechel, D. E., Gaskell, P. C., Small, G., … Pericak-Vance, M. A. (1993). Gene dose of apolipoprotein E type 4 allele and the risk of Alzheimer's disease in late onset families. *Science*, *261*, 921–923. https://doi.org/10.1126/science.8346443

Desai, M. K., Guercio, B. J., Narrow, W. C., & Bowers, W. J. (2011). An Alzheimer's disease-relevant presenilin-1 mutation augments amyloid-beta-induced oligodendrocyte dysfunction. *Glia*, *59*, 627–640. https://doi.org/10.1002/glia.21131

Desai, M. K., Mastrangelo, M. A., Ryan, D. A., Sudol, K. L., Narrow, W. C., & Bowers, W. J. (2010). Early oligodendrocyte/myelin pathology in Alzheimer's disease mice constitutes a novel therapeutic target. *The American Journal of Pathology*, *177*, 1422–1435. https://doi.org/10.2353/ajpath.2010.100087

Di Paolo, G., & Kim, T.-W. (2011). Linking lipids to Alzheimer's disease: Cholesterol and beyond. *Nature Reviews Neuroscience*, *12*, 284–296. https://doi.org/10.1038/nrn3012

Dufresne, M., Guneysu, D., Patterson, N. H., Marcinkiewicz, M. M., Regina, A., Demeule, M., & Chaurand, P. (2017). Multimodal detection of GM2 and GM3 lipid species in the brain of mucopolysaccharidosis type II mouse by serial imaging mass spectrometry and immunohistochemistry. *Analytical and Bioanalytical Chemistry*, *409*, 1425–1433. https://doi.org/10.1007/s00216-016-0076-x

Farooqui, A. A., Rapoport, S. I., & Horrocks, L. A. (1997). Membrane phospholipid alterations in Alzheimer's disease: Deficiency of ethanolamine plasmalogens. *Neurochemical Research*, *22*, 523–527.

Foley, P. (2010). Lipids in Alzheimer's disease: A century-old story. *Biochimica Et Biophysica Acta (BBA) – Molecular and Cell Biology of Lipids*, *1801*, 750–753. https://doi.org/10.1016/j.bbalip.2010.05.004

Ginsberg, L., Rafique, S., Xuereb, J. H., Rapoport, S. I., & Gershfeld, N. L. (1995). Disease and anatomic specificity of ethanolamine plasmalogen deficiency in Alzheimer's disease brain. *Brain Research*, *698*, 223–226. https://doi.org/10.1016/0006-8993(95)00931-F

Griciuc, A., Patel, S., Federico, A. N., Choi, S. H., Innes, B. J., Oram, M. K., … Tanzi, R. E. (2019). TREM2 Acts Downstream of CD33 in Modulating Microglial Pathology in Alzheimer's Disease. *Neuron*, *103*(5), 820–835.e7. https://doi.org/10.1016/j.neuron.2019.06.010

Grimm, M. O. W., Grimm, H. S., Pätzold, A. J., Zinser, E. G., Halonen, R., Duering, M., … Hartmann, T. (2005). Regulation of cholesterol and sphingomyelin metabolism by amyloid-β and presenilin. *Nature Cell Biology*, *7*, 1118–1123. https://doi.org/10.1038/ncb1313

Grimm, M. O. W., Kuchenbecker, J., Rothhaar, T. L., Grösgen, S., Hundsdörfer, B., Burg, V. K., … Hartmann, T. (2011). Plasmalogen synthesis is regulated via alkyl-dihydroxyacetonephosphate-synthase by amyloid precursor protein processing and is affected in Alzheimer's disease. *Journal of Neurochemistry*, *116*, 916–925. https://doi.org/10.1111/j.1471-4159.2010.07070.x

Hall, S. M. (1972). The effect of injections of lysophosphatidyl choline into white matter of the adult mouse spinal cord. *Journal of Cell Science*, *10*, 535–546.

Hamilton, L. K., Dufresne, M., Joppé, S. E., Petryszyn, S., Aumont, A., Calon, F., … Fernandes, K. J. L. (2015). Aberrant lipid metabolism in the forebrain niche suppresses adult neural stem cell proliferation in an animal model of Alzheimer's disease. *Cell Stem Cell*, *17*, 397–411. https://doi.org/10.1016/j.stem.2015.08.001

Han, X. (2007). Potential mechanisms contributing to sulfatide depletion at the earliest clinically recognizable stage of Alzheimer's disease: A tale of shotgun lipidomics. *Journal of Neurochemistry*, *103*, 171–179. https://doi.org/10.1111/j.1471-4159.2007.04708.x

Han, X., Cheng, H., Fryer, J. D., Fagan, A. M., & Holtzman, D. M. (2003). Novel role for apolipoprotein E in the central nervous system modulation of sulfatide content. *Journal of Biological Chemistry*, *278*, 8043–8051. https://doi.org/10.1074/jbc.M212340200

Han, X., Holtzman, D. M., & McKeel, D. W. (2001a). Plasmalogen deficiency in early Alzheimer's disease subjects and in animal models: Molecular characterization using electrospray ionization mass spectrometry. *Journal of Neurochemistry*, *77*, 1168–1180. https://doi.org/10.1046/j.1471-4159.2001.00332.x

Han, X., M. Holtzman, D., W. McKeel, D., Kelley, J., & Morris, J. C. (2002). Substantial sulfatide deficiency and ceramide elevation in very early Alzheimer's disease: Potential role in disease pathogenesis. *Journal of Neurochemistry*, *82*, 809–818. https://doi.org/10.1046/j.1471-4159.2002.00997.x

Hardy, J. A., & Higgins, G. A. (1992). Alzheimer's disease: The amyloid cascade hypothesis. *Science*, *256*, 184. https://doi.org/10.1126/science.1566067

Heneka, M. T., Carson, M. J., Khoury, J. E., Landreth, G. E., Brosseron, F., Feinstein, D. L., … Kummer, M. P. (2015). Neuroinflammation in Alzheimer's disease. *The Lancet Neurology*, *14*, 388–405. https://doi.org/10.1016/S1474-4422(15)70016-5

Hirahara, Y., Wakabayashi, T., Mori, T., Koike, T., Yao, I., Tsuda, M., … Yamada, H. (2017). Sulfatide species with various fatty acid chains in oligodendrocytes at different developmental stages determined by imaging mass spectrometry. *Journal of Neurochemistry*, *140*, 435–450. https://doi.org/10.1111/jnc.13897

Hong, I., Kang, T., Yoo, Y. C., Park, R., Lee, J., Lee, S., … Choi, S. (2013). Quantitative proteomic analysis of the hippocampus in the 5XFAD mouse model at early stages of Alzheimer's disease pathology. *Journal of Alzheimer's Disease*, *36*, 321–334. https://doi.org/10.3233/JAD-130311

Hong, J. H., Kang, J. W., Kim, D. K., Baik, S. H., Kim, K. H., Shanta, S. R., … Kim, K. P. (2016). Global changes of phospholipids identified by MALDI imaging mass spectrometry in a mouse model of Alzheimer's disease. *Journal of Lipid Research*, *57*, 36–45. https://doi.org/10.1194/jlr.M057869

Hunter, M., Demarais, N. J., Faull, R. L., Grey, A. C., & Curtis, M. A. (2018). Subventricular zone lipidomic architecture loss in Huntington's disease. *Journal of Neurochemistry*, *146*, 613–630. https://doi.org/10.1111/jnc.14468

Igarashi, M., Ma, K., Gao, F., Kim, H.-W., Rapoport, S. I., & Rao, J. S. (2011). Disturbed choline plasmalogen and phospholipid fatty acid concentrations in Alzheimer's disease prefrontal cortex. *Journal of Alzheimer's Disease*, *24*, 507–517. https://doi.org/10.3233/JAD-2011-101608

Isaac, G., Pernber, Z., Gieselmann, V., Hansson, E., Bergquist, J., & Månsson, J. E. (2006). Sulfatide with short fatty acid dominates in astrocytes and neurons. *The FEBS Journal*, *273*, 1782–1790. https://doi.org/10.1111/j.1742-4658.2006.05195.x

Jana, A., & Pahan, K. (2004). Fibrillar amyloid-β peptides kill human primary neurons via NADPH oxidase-mediated activation of neutral sphingomyelinase implications for Alzheimer's disease. *Journal of Biological Chemistry*, *279*, 51451–51459. https://doi.org/10.1074/jbc.M404635200

Katafuchi, T., Ifuku, M., Mawatari, S., Noda, M., Miake, K., Sugiyama, M., & Fujino, T. (2012). Effects of plasmalogens on systemic lipopolysaccharide-induced glial activation and β-amyloid accumulation in adult mice. *Annals of the New York Academy of Sciences*, *1262*, 85–92. https://doi.org/10.1111/j.1749-6632.2012.06641.x

Kaya, I., Brinet, D., Michno, W., Başkurt, M., Zetterberg, H., Blenow, K., … r., (2017a). Novel trimodal MALDI imaging mass spectrometry (IMS3) at 10 μm reveals spatial lipid and peptide correlates implicated in Aβ plaque pathology in Alzheimer's disease. *ACS Chemical Neuroscience*, *8*, 2778–2790. https://doi.org/10.1021/acschemneuro.7b00314

Kaya, I., Brinet, D., Michno, W., Syvänen, S., Sehlin, D., Zetterberg, H., … r., (2017b). Delineating amyloid plaque associated neuronal sphingolipids in transgenic Alzheimer's disease mice (tgArcSwe) using MALDI imaging mass spectrometry. *ACS Chemical Neuroscience*, *8*, 347–355. https://doi.org/10.1021/acschemneuro.6b00391

Kaya, I., Jennische, E., Dunevall, J., Lange, S., Ewing, A. G., Malmberg, P., … Fletcher, J. S. (2019). Spatial lipidomics reveals region and long chain base specific accumulations of monosialogangliosides in amyloid plaques in familial Alzheimer's disease mice (5xFAD) brain. *ACS Chemical Neuroscience*, *11*, 14–24. https://doi.org/10.1021/acschemneuro.9b00532

Kaya, I., Jennische, E., Lange, S., & Malmberg, P. (2018a). Dual polarity MALDI imaging mass spectrometry on the same pixel points reveals spatial lipid localizations at high-spatial resolutions in rat small intestine. *Analytical Methods*, *10*, 2428–2435. https://doi.org/10.1039/C8AY00645H

Kaya, I., Michno, W., Brinet, D., Iacone, Y., Zanni, G., Blennow, K., … r., (2017c). Histology-compatible MALDI mass spectrometry based imaging of neuronal lipids for subsequent immunofluorescent staining. *Analytical Chemistry*, *89*, 4685–4694. https://doi.org/10.1021/acs.analchem.7b00313

Kaya, I., Zetterberg, H., Blennow, K., Hanrieder, J., & r., (2018b). Shedding light on the molecular pathology of amyloid plaques in transgenic Alzheimer's disease mice using multimodal MALDI imaging mass spectrometry. *ACS Chemical Neuroscience*, *9*, 1802–1817. https://doi.org/10.1021/acschemneuro.8b00121

Kim, J., Basak, J. M., & Holtzman, D. M. (2009). The role of apolipoprotein E in Alzheimer's disease. *Neuron*, *63*, 287–303. https://doi.org/10.1016/j.neuron.2009.06.026

Kou, J., Kovacs, G. G., Höftberger, R., Kulik, W., Brodde, A., Forss-Petter, S., … Berger, J. (2011). Peroxisomal alterations in Alzheimer's disease. *Acta Neuropathologica*, *122*, 271–283. https://doi.org/10.1007/s00401-011-0836-9

Lacor, P. N., Buniel, M. C., Chang, L., Fernandez, S. J., Gong, Y., Viola, K. L., … Krafft, G. A. (2004). Synaptic targeting by Alzheimer's-related amyloid β oligomers. *Journal of Neuroscience*, *24*, 10191–10200.

Lee, C. Y. D., Daggett, A., Gu, X., Jiang, L.-L., Langfelder, P., Li, X., … Yang, X. W. (2018). Elevated TREM2 gene dosage reprograms microglia responsivity and ameliorates pathological phenotypes in Alzheimer's disease models. *Neuron*, *97*(5), 1032–1048.e5. https://doi.org/10.1016/j.neuron.2018.02.002

Lee, J.-T., Xu, J., Lee, J.-M., Ku, G., Han, X., Yang, D.-I., … Hsu, C. Y. (2004). Amyloid-β peptide induces oligodendrocyte death by activating the neutral sphingomyelinase–ceramide pathway. *The Journal of Cell Biology*, *164*, 123–131. https://doi.org/10.1083/jcb.200307017

Mallah, K., Quanico, J., Trede, D., Kobeissy, F., Zibara, K., Salzet, M., & Fournier, I. (2018). Lipid changes associated with traumatic brain injury revealed by 3D MALDI-MSI. *Analytical Chemistry*, *90*, 10568–10576. https://doi.org/10.1021/acs.analchem.8b02682

McDonnell, L. A., & Heeren, R. (2007). Imaging mass spectrometry. *Mass Spectrometry Reviews*, *26*, 606–643. https://doi.org/10.1002/mas.20124

Michno, W., Kaya, I., Nyström, S., Guerard, L., Nilsson, K. P. R., Hammarström, P., … Hanrieder, J. (2018). Multimodal chemical imaging of amyloid plaque polymorphism reveals Aβ aggregation dependent anionic lipid accumulations and metabolism. *Analytical Chemistry*, *90*, 8130–8138. https://doi.org/10.1021/acs.analchem.8b01361

Mitew, S., Kirkcaldie, M. T., Halliday, G. M., Shepherd, C. E., Vickers, J. C., & Dickson, T. C. (2010). Focal demyelination in Alzheimer's disease and transgenic mouse models. *Acta Neuropathologica*, *119*, 567–577. https://doi.org/10.1007/s00401-010-0657-2

Möller, H.-J., & Graeber, M. (1998). The case described by Alois Alzheimer in 1911. *European Archives of Psychiatry and Clinical Neuroscience*, *248*, 111–122. https://doi.org/10.1007/s004060050027

Nakai, M., Kawamata, T., Taniguchi, T., Maeda, K., & Tanaka, C. (1996). Expression of apolipoprotein E mRNA in rat microglia. *Neuroscience Letters*, *211*, 41–44. https://doi.org/10.1016/0304-3940(96)12716-6

Nasrabady, S. E., Rizvi, B., Goldman, J. E., & Brickman, A. M. (2018). White matter changes in Alzheimer's disease: A focus on myelin and oligodendrocytes. *Acta Neuropathologica Communications*, *6*, 22. https://doi.org/10.1186/s40478-018-0515-3

Norton, W., & Poduslo, S. (1973). Myelination in rat brain: Changes in myelin composition during brain maturation. *Journal of Neurochemistry*, *21*, 759–773. https://doi.org/10.1111/j.1471-4159.1973.tb07520.x

Oakley, H., Cole, S. L., Logan, S. *et al.* (2006). Intraneuronal β-amyloid aggregates, neurodegeneration, and neuron loss in transgenic mice with five familial Alzheimer's disease mutations: Potential factors in amyloid plaque formation. *Journal of Neuroscience*, *26*, 10129–10140.

Palavicini, J. P., Wang, C., Chen, L., Hosang, K., Wang, J., Tomiyama, T., … Han, X. (2017). Oligomeric amyloid-beta induces MAPK-mediated activation of brain cytosolic and calcium-independent phospholipase A 2 in a spatial-specific manner. *Acta Neuropathologica Communications*, *5*, 56. https://doi.org/10.1186/s40478-017-0460-6

Palop, J. J., & Mucke, L. (2010). Amyloid-β–induced neuronal dysfunction in Alzheimer's disease: From synapses toward neural networks. *Nature Neuroscience*, *13*, 812. https://doi.org/10.1038/nn.2583

Plemel, J. R., Michaels, N. J., Weishaupt, N., Caprariello, A. V., Keough, M. B., Rogers, J. A., … Yong, V. W. (2018). Mechanisms of lysophosphatidylcholine-induced demyelination: A primary lipid disrupting myelinopathy. *Glia*, *66*, 327–347. https://doi.org/10.1002/glia.23245

Rangaraju, S., Dammer, E. B., Raza, S. A., Gao, T., Xiao, H., Betarbet, R., … Seyfried, N. T. (2018). Quantitative proteomics of acutely-isolated mouse microglia identifies novel immune Alzheimer's disease-related proteins. *Molecular Neurodegeneration*, *13*, 34. https://doi.org/10.1186/s13024-018-0266-4

Saunders, A. M., Strittmatter, W. J., Schmechel, D., George-Hyslop, P. S., Pericak-Vance, M. A., Joo, S. H., … Hulette, C. (1993). Association of apolipoprotein E allele ϵ4 with late-onset familial and sporadic Alzheimer's disease. *Neurology*, *43*, 1467–1467.

Stoeckli, M., Staab, D., Staufenbiel, M., Wiederhold, K.-H., & Signor, L. (2002). Molecular imaging of amyloid β peptides in mouse brain sections using mass spectrometry. *Analytical Biochemistry*, *311*, 33–39. https://doi.org/10.1016/S0003-2697(02)00386-X

Strittmatter, W. J., Saunders, A. M., Schmechel, D., Pericak-Vance, M., Enghild, J., Salvesen, G. S., & Roses, A. D. (1993). Apolipoprotein E: High-avidity binding to beta-amyloid and increased frequency of type 4 allele in late-onset familial Alzheimer disease. *Proceedings of the National Academy of Sciences of the United States of America*, *90*, 1977–1981. https://doi.org/10.1073/pnas.90.5.1977

Su, X. Q., Wang, J., & Sinclair, A. J. (2019). Plasmalogens and Alzheimer's disease: A review. *Lipids in Health and Disease*, *18*, 100. https://doi.org/10.1186/s12944-019-1044-1

Thomas, A., Charbonneau, J. L., Fournaise, E., & Chaurand, P. (2012). Sublimation of new matrix candidates for high spatial resolution imaging mass spectrometry of lipids: Enhanced information in both positive and negative polarities after 1, 5-diaminonapthalene deposition. *Analytical Chemistry*, *84*, 2048–2054. https://doi.org/10.1021/ac2033547

Tobias, F., Pathmasiri, K. C., & Cologna, S. M. (2019). Mass spectrometry imaging reveals ganglioside and ceramide localization patterns during cerebellar degeneration in the Npc1$^{-/-}$ mouse model. *Analytical and Bioanalytical Chemistry*, *411*, 5659–5668. https://doi.org/10.1007/s00216-019-01989-7

Ulland, T. K., Song, W. M., Huang, S.-C., Ulrich, J. D., Sergushichev, A., Beatty, W. L., … Colonna, M. (2017). TREM2 maintains microglial metabolic fitness in Alzheimer's disease. *Cell*, *170*(4), 649–663.e13. https://doi.org/10.1016/j.cell.2017.07.023

Wang, C., Palavicini, J. P., & Han, X. (2018). Lipidomics profiling of myelin. In: A. Woodhoo (Ed.), *Myelin* (pp. 37–50). Berlin, Germany: Springer.

Wang, Y., Cella, M., Mallinson, K., Ulrich, J. D., Young, K. L., Robinette, M. L., … Colonna, M. (2015). TREM2 lipid sensing sustains the microglial response in an Alzheimer's disease model. *Cell*, *160*, 1061–1071. https://doi.org/10.1016/j.cell.2015.01.049

Wang, Y., Ulland, T. K., Ulrich, J. D., Song, W., Tzaferis, J. A., Hole, J. T., … Colonna, M. (2016). TREM2-mediated early microglial response limits diffusion and toxicity of amyloid plaques. *Journal of Experimental Medicine*, *jem*, 20151948. https://doi.org/10.1084/jem.20151948

Whiley, L., Sen, A., Heaton, J., Proitsi, P., García-Gómez, D., Leung, R., … Legido-Quigley, C. (2014). Evidence of altered phosphatidylcholine metabolism in Alzheimer's disease. *Neurobiology of Aging*, *35*, 271–278. https://doi.org/10.1016/j.neurobiolaging.2013.08.001

Woods, A. S., Colsch, B., Jackson, S. N., Post, J., Baldwin, K., Roux, A., … Balaban, C. (2013). Gangliosides and ceramides change in a mouse model of blast induced traumatic brain injury. *ACS Chemical Neuroscience*, *4*, 594–600. https://doi.org/10.1021/cn300216h

Xu, J., Chen, S., Ahmed, S. H., Chen, H., Ku, G., Goldberg, M. P., & Hsu, C. Y. (2001). Amyloid-β peptides are cytotoxic to oligodendrocytes. *Journal of Neuroscience*, *21*, RC118–RC118. https://doi.org/10.1523/JNEUROSCI.21-01-j0001.2001

Yang, D.-S., Stavrides, P., Saito, M., Kumar, A., Rodriguez-Navarro, J. A., Pawlik, M., … Nixon, R. A. (2014). Defective macroautophagic turnover of brain lipids in the TgCRND8 Alzheimer mouse model: Prevention by correcting lysosomal proteolytic deficits. *Brain*, *137*, 3300–3318. https://doi.org/10.1093/brain/awu278

Yuki, D., Sugiura, Y., Zaima, N., Akatsu, H., Takei, S., Yao, I., … Setou, M. (2014). DHA-PC and PSD-95 decrease after loss of synaptophysin and before neuronal loss in patients with Alzheimer's disease. *Scientific Reports*, *4*, 7130. https://doi.org/10.1038/srep07130

Zemski Berry, K. A., Hankin, J. A., Barkley, R. M., Spraggins, J. M., Caprioli, R. M., & Murphy, R. C. (2011). MALDI imaging of lipid biochemistry in tissues by mass spectrometry. *Chemical Reviews*, *111*, 6491–6512. https://doi.org/10.1021/cr200280p

SUPPORTING INFORMATION

Additional supporting information may be found online in the Supporting Information section.

How to cite this article: Kaya I, Jennische E, Lange S, Tarik Baykal A, Malmberg P, Fletcher JS. Brain region-specific amyloid plaque-associated myelin lipid loss, APOE deposition and disruption of the myelin sheath in familial Alzheimer's disease mice. *J Neurochem*. 2020;00:1–15. https://doi.org/10.1111/jnc.14999